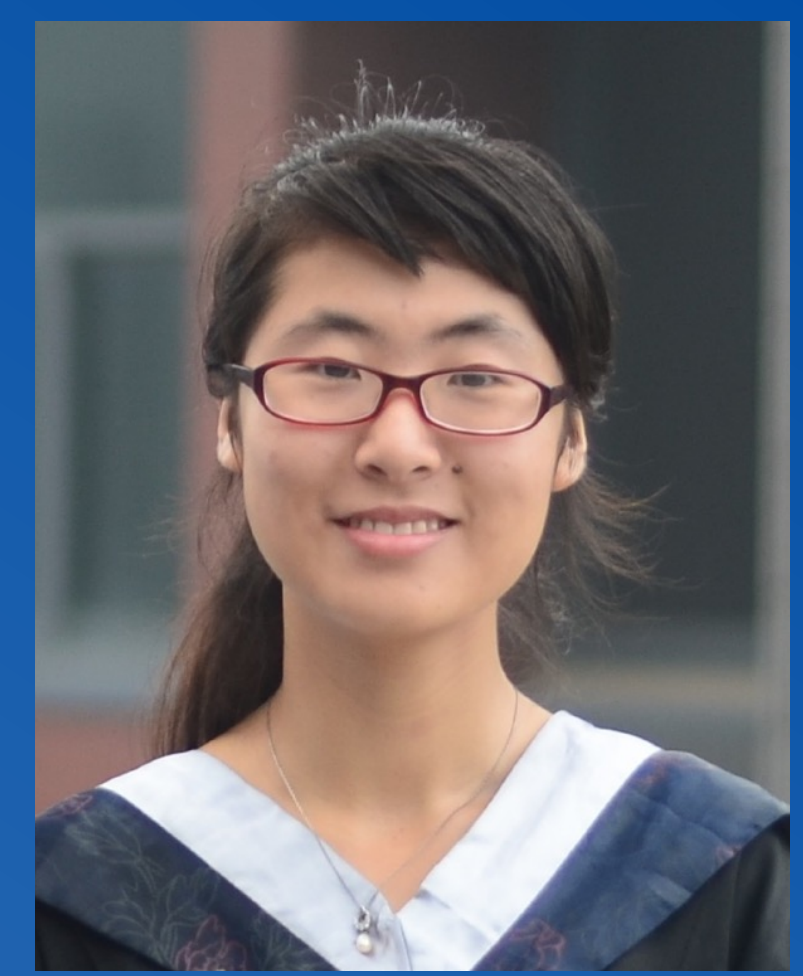


The SOFIA Massive (SOMA) Star Formation Survey - Peering to the Heart of Massive Star Birth

Mengyao Liu¹, Jonathan C. Tan¹, James M. De Buizer², Yichen Zhang^{3,4}, Maria Beltrán⁵, Ralph Shuping², Jan Staff^{1,6}, Kei Tanaka¹, and Barbara Whitney⁷
¹UF, ²SOFIA, ³U. Chile, ⁴RIKEN, ⁵Arcetri, ⁶UVI, ⁷UW



Abstract

Massive star formation remains an important unsolved problem in astrophysics. A detailed multi-wavelength comparison between theoretical models and observations of massive protostars will help advance our understanding of the massive star formation process. Here we present results of the SOFIA Massive (SOMA) star formation survey, which aims to build up a sample of ~ 50 massive and intermediate-mass protostars in a range of different environments that are observed across MIR and FIR bands to test theoretical models of massive star formation. We build the spectral energy distributions (SEDs) of massive and intermediate-mass protostars observed with *SOFIA-FORCAST* from ~ 10 to $40 \mu\text{m}$ together with archival *Spitzer* and *Herschel* data and other ground-based IR data. Radiation transfer (RT) models of Zhang & Tan (ZT, in prep.), which are based on the Core Accretion scenario, including outflow cavities driven by MHD disk winds, are then fit to the SEDs. As a comparison, we also fit the SEDs with the widely used Robitaille et al. (2007) models. We examine to what extent these simple, symmetric core accretion models can fit these protostellar sources and the different results that are obtained by using different model grids.

1. Introduction

Massive stars impact many areas of astrophysics, yet there is still no consensus on how they form. One possible scenario is the **Turbulent Core Accretion** model (McKee & Tan 2002, 2003), which may involve relatively ordered, monolithic accretion via a central disk and the driving of collimated bipolar outflows. Outflows may limit the formation efficiency since they expel material along polar directions. The resulting **outflow cavities** have been proposed to significantly affect the appearance of the protostar in the **mid-IR (MIR)** (De Buizer 2006) and this is seen in the **RT calculations** using the RT code.

2. SOFIA Massive (SOMA) Star Formation Survey

The SOFIA Massive (SOMA) star formation survey aims to obtain ~ 10 to $40 \mu\text{m}$ images of a statistically significant sample of about **50 high- and intermediate-mass protostars** over a range of evolutionary stages and then compare the observed **SEDs** and **image intensity profiles** with theoretical models. MIR to FIR *SOFIA-FORCAST* observations have been carried out in Basic Science and Cycles 1-4. The MIR emission is expected to be a powerful tracer of heated dust in protostellar outflow cavities (De Buizer 2006; Zhang et al. 2013). **15** sources have been observed and **8** more are expected to be completed by the end of Cycle 4.

3. SED Fitting with RT Models

We build spectral energy distributions (SEDs) of the first eight sources in the SOMA survey from $3.6 \mu\text{m}$ up to $500 \mu\text{m}$ with photometric data of *Spitzer*, *IRTF*, *Gemini*, *SOFIA* and *Herschel*. We use PHOTUTILS, a PYTHON package to measure the flux photometry. Then we fit the fiducial SEDs (with fixed aperture and with background subtraction) with both **ZT (in prep.) RT models** (see Figure 1) and **Robitaille et al. (2007) RT models**. The fitting results are shown in Figure 2. The key parameters of the best fitting models are listed in Table 1. Table 2 shows the best 5 ZT models of G35.20-0.74 as an example to illustrate the fitting preference and the variation in all model parameters.

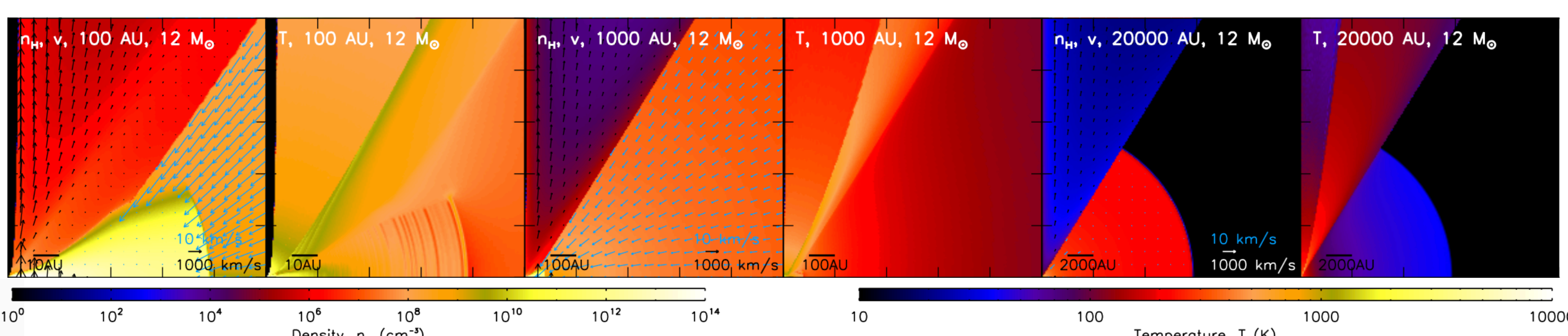


Figure 1. Input density and converged temperature profiles for the fiducial model ($M_c = 60 M_\odot$, $\Sigma_{\text{cl}} = 1 \text{ g/cm}^2$, $\beta_c = 0.02$) with $m^* = 12 M_\odot$ (Zhang et al. 2014).

Table 1. Parameters of the Best Fitted Model of Zhang & Tan and Robitaille et al.

| Source | χ^2/N | M_c (M_\odot) | Σ_{cl} (g cm^{-2}) | Zhang & Tan models | | | | | | Robitaille et al. models | | | | | | | | |
|-------------|------------|------------------------|--|------------------------|---------------------------------|----------------|-----------------------------------|----------------------------------|--|-----------------------------------|------------|------------------------|---------------------------------|----------------|----------------------------------|---|--|-----------------------------------|
| | | | | m_* (M_\odot) | θ_{view} (deg) | A_V (mag) | M_{env} (M_\odot) | $\theta_{w,\text{esc}}$ (deg) | \dot{M}_{disk} (M_\odot/yr) | L_{bol} (L_\odot) | χ^2/N | m_* (M_\odot) | θ_{view} (deg) | A_V (mag) | $\theta_{w,\text{esc}}$ (deg) | M_{env} (M_\odot/yr) | \dot{M}_{disk} (M_\odot/yr) | L_{bol} (L_\odot) |
| AFGL4029 | 3.4 | 30 | 1.0 | 12 | 62 | 0.1 | 6 | 53 | 1.9×10^{-4} | 4.2×10^4 | 1.8 | 13 | 18 | 55.2 | 42 | 1.7×10^{-4} | 4.4×10^{-7} | 1.2×10^4 |
| AFGL437 | 2.6 | 50 | 3.2 | 8 | 29 | 0.1 | 35 | 25 | 6.0×10^{-4} | 1.7×10^4 | 0.8 | 15 | 87 | 15.7 | 35 | 2.9×10^{-4} | 9.7×10^{-6} | 2.3×10^4 |
| IRAS07299 | 1.4 | 60 | 0.3 | 12 | 77 | 9.3 | 32 | 40 | 1.2×10^{-4} | 2.8×10^4 | 1.1 | 18 | 76 | 13.2 | 10 | 4.3×10^{-4} | ... | 8.3×10^3 |
| G35.20-0.74 | 4.3 | 120 | 3.2 | 12 | 29 | 37.6 | 99 | 18 | 9.6×10^{-4} | 5.4×10^4 | 2.3 | 20 | 87 | 20.7 | 34 | 1.6×10^{-3} | 2.8×10^{-7} | 4.7×10^4 |
| G45.47+0.05 | 3.5 | 240 | 1.0 | 32 | 86 | 15.2 | 170 | 30 | 7.2×10^{-4} | 2.7×10^5 | 3.4 | 31 | 57 | 16.8 | 20 | 4.1×10^{-3} | ... | 1.4×10^5 |
| IRAS20126 | 2.3 | 120 | 0.3 | 24 | 86 | 61.4 | 57 | 47 | 1.8×10^{-4} | 9.5×10^4 | 1.1 | 18 | 87 | 87.1 | 17 | 4.4×10^{-4} | 5.7×10^{-7} | 2.3×10^4 |
| CepA | 4.9 | 480 | 0.1 | 12 | 83 | 81.1 | 458 | 12 | 1.0×10^{-4} | 2.4×10^4 | 1.5 | 15 | 49 | 64.3 | 15 | 1.3×10^{-3} | 8.1×10^{-6} | 2.9×10^4 |
| NGC7538 | 0.6 | 480 | 0.1 | 16 | 22 | 9.3 | 441 | 15 | 1.2×10^{-4} | 3.9×10^4 | 0.3 | 17 | 18 | 44.9 | 15 | 1.5×10^{-3} | 4.2×10^{-6} | 2.6×10^4 |

Table 2. Parameters of the Best 5 Fitted Models of Zhang & Tan for G35.20-0.74

| Source | χ^2/N | M_c (M_\odot) | Σ_{cl} (g cm^{-2}) | Zhang & Tan models | | | | | | Robitaille et al. models | | | | | | | | |
|-------------|------------|------------------------|--|------------------------|---------------------------------|----------------|-----------------------------------|----------------------------------|--|-----------------------------------|------------|------------------------|---------------------------------|----------------|----------------------------------|---|--|-----------------------------------|
| | | | | m_* (M_\odot) | θ_{view} (deg) | A_V (mag) | M_{env} (M_\odot) | $\theta_{w,\text{esc}}$ (deg) | \dot{M}_{disk} (M_\odot/yr) | L_{bol} (L_\odot) | χ^2/N | m_* (M_\odot) | θ_{view} (deg) | A_V (mag) | $\theta_{w,\text{esc}}$ (deg) | M_{env} (M_\odot/yr) | \dot{M}_{disk} (M_\odot/yr) | L_{bol} (L_\odot) |
| G35.20-0.74 | 4.3 | 120 | 3.2 | 12 | 29 | 37.6 | 99 | 18 | 9.6×10^{-4} | 5.4×10^4 | 2.3 | 20 | 87 | 20.7 | 34 | 1.6×10^{-3} | 2.8×10^{-7} | 4.7×10^4 |
| | 8.0 | 120 | 1.0 | 24 | 48 | 57.2 | 68 | 37 | 4.9×10^{-4} | 1.5×10^5 | 2.4 | 20 | 81 | 24.1 | 34 | 1.6×10^{-3} | 2.8×10^{-7} | 4.7×10^4 |
| | 8.0 | 120 | 1.0 | 12 | 29 | 3.5 | 96 | 20 | 4.0×10^{-4} | 5.0×10^4 | 2.5 | 20 | 76 | 33.0 | 34 | 1.6×10^{-3} | 2.8×10^{-7} | 4.7×10^4 |
| | 9.8 | 60 | 3.2 | 16 | 48 | 81.1 | 31 | 32 | 8.4×10^{-4} | 1.2×10^5 | 2.5 | 19 | 70 | 16.4 | 27 | 1.5×10^{-3} | 2.6×10^{-7} | 4.3×10^4 |
| | 10.8 | 60 | 3.2 | 12 | 48 | 7.1 | 38 | 27 | 7.6×10^{-4} | 5.2×10^4 | 2.7 | 18 | 76 | 16.8 | 29 | 1.2×10^{-3} | 3.9×10^{-6} | 3.6×10^4 |

Table 3. Parameters of the Best Fitted Models of Zhang & Tan for different SEDs of AFGL4029

| Source | χ^2/N | M_c (M_\odot) | Σ_{cl} (g cm^{-2}) | m_* (M_\odot) | θ_{view} (deg) | A_V (mag) | M_{env} (M_\odot) | $\theta_{w,\text{esc}}$ (deg) | \dot{M}_{disk} (M_\odot/yr) | L_{bol} (L_\odot) |
|-----------------------|------------|------------------------|--|------------------------|---------------------------------|----------------|-----------------------------------|----------------------------------|--|-----------------------------------|
| AFGL4029 ^a | 3.4 | 30 | 1.0 | 12 | 62 | 0.1 | 6 | 53 | 1.9×10^{-4} | 4.2×10^4 |
| b | 2.1 | 120 | 0.1 | 24 | 89 | 40.4 | 42 | 57 | 6.3×10^{-5} | 7.5×10^4 |
| c | 2.7 | 30 | 1.0 | 12 | 62 | 5.0 | 6 | 53 | 1.9×10^{-4} | 4.2×10^4 |
| d | 1.9 | 120 | 0.1 | 24 | 89 | 46.4 | 42 | 57 | 6.3×10^{-5} | 7.5×10^4 |

^aFlux density derived with fixed aperture and with background subtraction.
^bFlux density derived with fixed aperture and without background subtraction.
^cFlux density derived with variable aperture and with background subtraction.
^dFlux density derived with variable aperture and without background subtraction.

References

De Buizer, J. M., 2006, ApJ, 642, L57; McKee, C. F., & Tan, J. C. 2002, Natur, 416, 59; McKee, C. F., & Tan, J. C. 2003, ApJ, 585, 850; Robitaille, T. P., Whitney, B. A., Indebetouw, R., & Wood, K. 2007, ApJS, 169, 328; Zhang Y., Tan J. C. et al. 2013b, ApJ, 767, 58.; Zhang, Y., Tan, J. C., & Hosokawa, T. 2014, ApJ, 788, 166.

4. Conclusions and Future Work

- The 8 sources tend to show extended MIR emission that **aligns** with known outflows, and being **brighter on the near-facing, blue-shifted side**, which are predictions of Turbulent Core Accretion models.
- The fiducial SEDs have been used to constrain theoretical RT models of massive star formation via the Turbulent Core Accretion model. These yield protostellar masses $m^* \sim 10\text{-}30 M_\odot$ accreting at rates of $\dot{M}_{\text{disk}} \sim 10^{-4}\text{-}10^{-3} M_\odot/\text{yr}$ inside cores of initial masses $M_c \sim 30\text{-}500 M_\odot$ embedded in clumps with mass surface densities $\Sigma_{\text{cl}} \sim 0.1\text{-}3 \text{ g/cm}^2$.
- Robitaille et al. (2007) model grid tend to give **much lower disk accretion rates** than ZT models: typically ~ 100 times smaller. In some cases, the models do not require any disk component.
- Future work will present **additional sources** (see Figure 3). Additional analysis that examines and models **flux profiles** along outflow cavity axes will be carried out, following methods developed by Zhang et al. (2013b). **Ancillary observations** that trace the outflowing gas will also be presented.

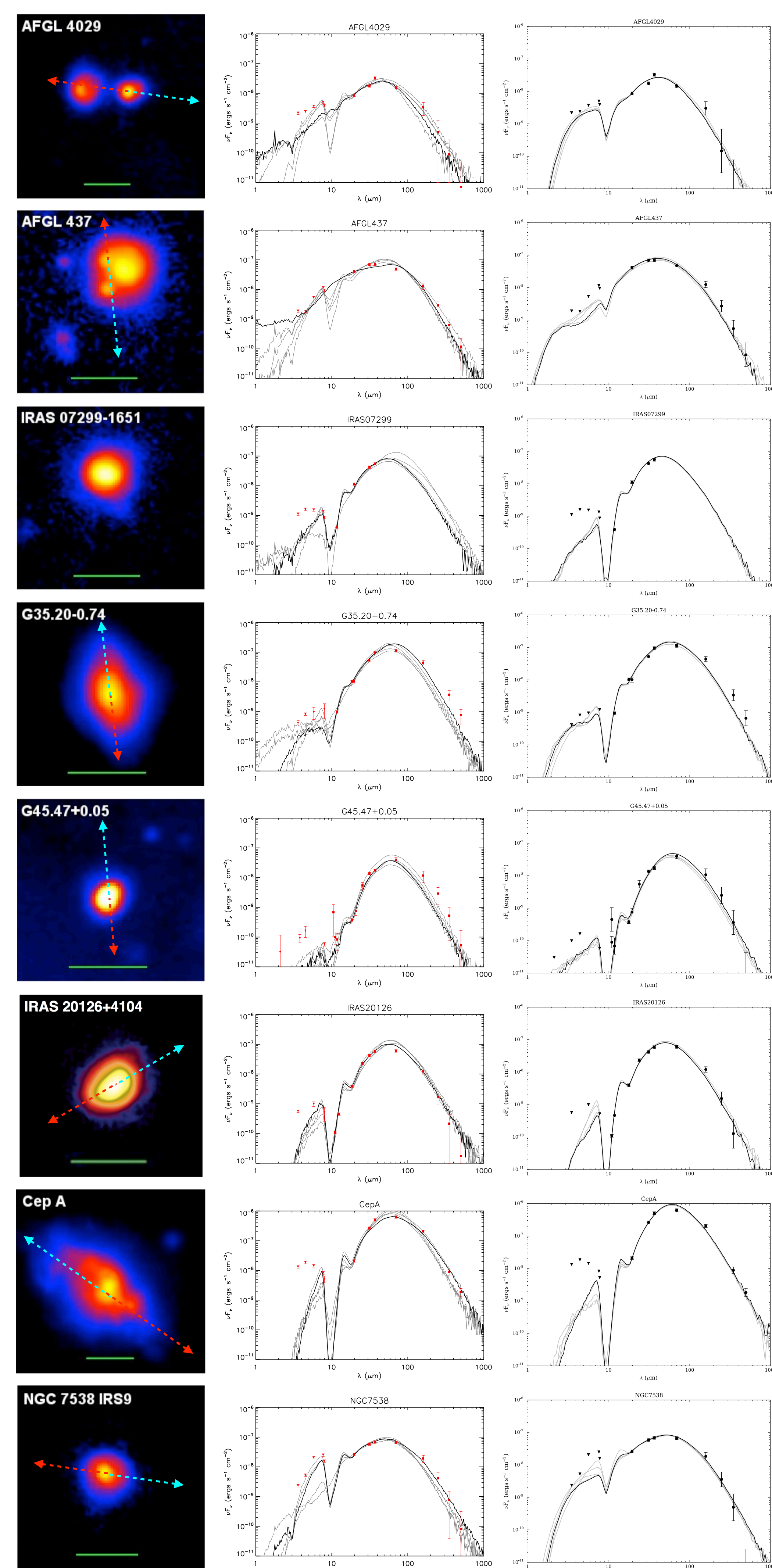


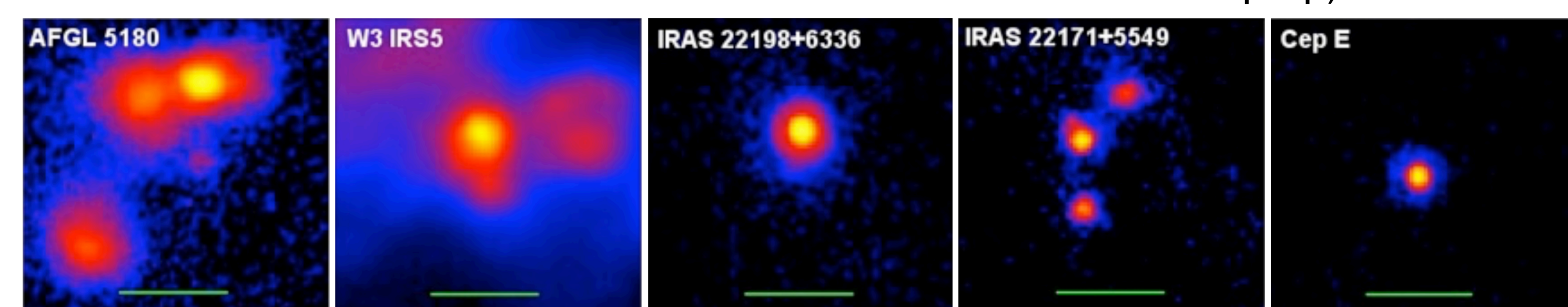
Figure 2.

Left - *SOFIA-FORCAST* observation of the first 8 massive and intermediate-mass protostars at $37 \mu\text{m}$. The scale bar is $30''$. The blue and red arrows indicate outflow directions from literature.

Middle - SED fit to the measured flux densities using the models of ZT. The top 5 best models are shown. We treat flux at wavelength $< 8 \mu\text{m}$ as upper limit. The error bars are set to be the larger of either 10% of the background subtracted flux density or the value of the estimated background flux density.

Right - Same with Middle but using the models of Robitaille et al. (2007). Note that the fitting method sets the data point to be at the middle of the error bar range.

Figure 3. *SOFIA-FORCAST* observation of the SOMA survey sample at $37 \mu\text{m}$. The scale bar is $30''$. (Liu et al. in prep)



We also explore the effect of **aperture size** and **background subtraction** on SED fitting. We show the fitting results of AFGL4029 with ZT models as an example in Table 3.